ACS Catalysis

Research Article

pubs.acs.org/acscatalysis

Pd_xCo_y Nanoparticle/Carbon Nanofiber Composites with Enhanced Electrocatalytic Properties

Dong Liu,[†] Qiaohui Guo,[†] Haoqing Hou,[‡] Osamu Niwa,[§] and Tianyan You*[,†]

[†]State Key Laboratory of Electroanalytical Chemistry, Changchun Institute of Applied Chemistry, Chinese Academy of Sciences, 5625 Renmin Street, Changchun, Jilin 130022, China

[‡]College of Chemistry and Chemical Engineering, Jiangxi Normal University, Jiangxi 330027, China

[§]Nano-biodevice Research Group, Biomedical Research Institute, National Institute of Advanced Industrial Science and Technology, Central 6, 1-1-1 Higashi, Tsukuba, Ibaraki 305-8566, Japan

Supporting Information

ABSTRACT: Novel bimetallic Pd_xCo_y alloy nanoparticle (NP)/carbon nanofiber (CNF) composites with superior electrocatalytic performances were successfully prepared by electrospinning Pd and Co precursors, i.e., $Pd(acac)_2$ and $Co(acac)_2$, in polyacrylonitrile followed by a thermal treatment. Uniform dispersion of Pd_xCo_y nanoparticles in carbon nanofibers was achieved. Chemical composition and size of the resulting Pd_xCo_y NPs, which showed a substantial effect on the electrocatalytic properties of Pd_xCo_y/CNF nanocomposites, can be readily controlled by adjusting the feed ratio of metal precursors. In comparison with commercial Pd/C and other state-of-the-art Pd- or Pt-based catalysts, Pd_xCo_y/CNF nanocomposites prepared in this study exhibited much higher electrocatalytic activity and stability in formic acid and methanol oxidation reactions. This improved electrocatalytic performance is very attractive for fuel cell applications and can be attributed to the unique bimetallic Pd−Co alloy formation, a modified electronic structure of Pd in Pd_xCo_y, as well as uniform dispersion and firm embedment of Pd_xCo_y NPs in CNF.

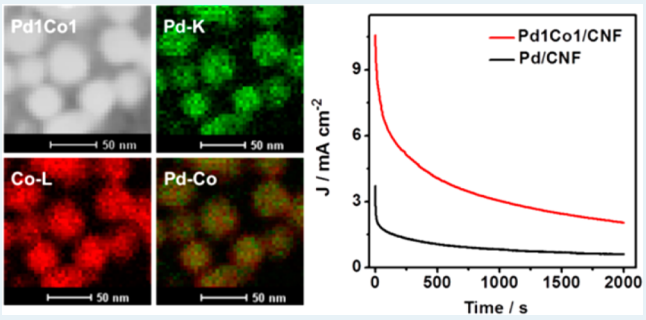

KEYWORDS: *Pd_xCo_y, alloy nanoparticle, embedded nanostructure, carbon nanofibers, formic acid oxidation*

INTRODUCTION

Direct liquid fuel cells, such as direct formic acid fuel cells (DFAFCs) and direct methanol fuel cells (DMFCs), are attracting more and more attention as new generation power sources.[1−4] Traditionally, Pt-based nanomaterials have been used as catalysts in fuel cells.[5,6] However, high-cost and carbon monoxide (CO) poisoning associated with Pt catalysts limit their practical applications. Recently, Pd-based catalysts, particularly Pd-transition metal alloys, have emerged as an alternative to Pt-based catalysts due to their good resistance to CO poisoning, high catalytic activity, and low cost.[3,4,7−10]

Meanwhile, preparation of carbon-supported Pd catalysts appears as an effective approach toward anode catalysts for low-temperature fuel cell applications.[8,11] Carbon blacks, such as acetylene black, Vulcan XC-72, and ketjen black, have been widely used as supporting materials. However, these amorphous carbon supports are vulnerable to corrosion/oxidation and tend to result in electrical isolation of catalyst nanoparticles (NPs). Pd catalysts are typically loosely absorbed on supporting carbon blacks; interaction between the two is fairly weak.[12] Detachment, aggregation, and even dissolution of NPs may occur during potential cycling, leading to degradation in performance.[13] In comparison, carbon supports with a higher degree of graphitization, e.g., carbon nanotube,[14] carbon nanofiber,[15] graphene,[16] and mesoporous graphitic carbon,[17] have shown improved resistance to corrosion. To achieve good electrocatalytic performance, however, these presynthesized carbon supports need to be purified and/or surface functionalized, which may damage the framework and decrease the electrical conductivity.[18,19] Complexity in multistep preparation typically required for such carbon-supported catalysts makes it difficult to produce these catalysts on a large scale. Thus, for practical fuel cell applications, it is highly desired to develop a simple and efficient process for preparing carbon-supported Pd catalysts with excellent electrocatalytic properties.

Herein, we report a facile preparation method for a new type of carbon-supported Pd catalyst, i.e., Pd−Co alloy NP/carbon nanofiber (Pd_xCo_y/CNF) composites, by using electrospinning and thermal treatment techniques. In the composites, Pd_xCo_y NPs are uniformly dispersed in the carbon nanofiber matrix, rather than weakly absorbed on the surface. Such an "embedded nanostructure" was deemed capable of yielding

Received: January 6, 2014
Revised: April 1, 2014
Published: April 24, 2014

   dx.doi.org/10.1021/cs5000153 | ACS Catal. 2014, 4, 1825−1829

highly active and stable catalysts. To realize such a nanocomposite, Pd and Co precursors, i.e., palladium(II) acetylacetonate ($Pd(acac)_2$), and cobalt(II) acetylacetonate ($Co(acac)_2$), with different Pd/Co molar feed ratios in range of 2:1 to 1:2 were mixed with a CNF precursor, i.e., polyacrylonitrile (PAN), and electrospun into the nanofiber. After carbonization at 850 °C, Pd_xCo_y/CNF nanocomposites were obtained, with Pd_xCo_y NPs formed in situ being tightly embedded in the CNF matrix. In such a structure, the CNF serves not only as a conductive carbon support but also as a solid barrier to prevent NPs from aggregation. The size and chemical composition of Pd_xCo_y NPs can be readily controlled by adjusting the Pd/Co feed ratio. Because the Pd_xCo_y NPs were formed in situ simultaneously with the formation of CNF, the preparation of Pd_xCo_y/CNF composites is regarded as a one-step process, which allows easy quality control, good reproducibility, and cost-effectiveness. Electrochemical properties and catalytic performance of the resulting Pd_xCo_y/CNF composites in formic acid and methanol oxidation were carefully evaluated, which showed superior properties, particularly in terms of catalytic activity and stability, than most state-of-the-art Pt- or Pd-based catalysts. This suggests a good potential of these new Pd_xCo_y/CNF composites in fuel cell applications.

RESULTS AND DISCUSSION

Figure 1 shows typical scanning electron microscopy (SEM) and transmission electron microscopy (TEM) pictures of

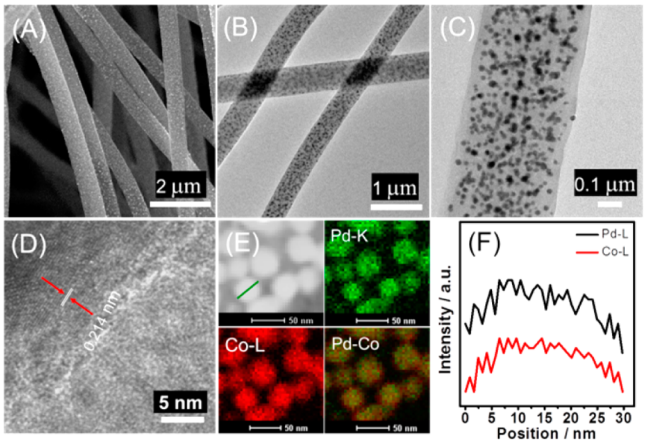

Figure 1. SEM (A), TEM (B, C), HRTEM (D), and STEM-HAADF (E) images and STEM-EDX line scan profile (F) of Pd_1Co_1/CNF nanocomposite.

Pd_1Co_1 NP/CNF composites obtained at a Pd/Co feed ratio of 1/1. The diameter of CNF in the composite ranges from 300 to 500 nm, and length in the scale of tens of micrometers. Pd_1Co_1 alloy NPs, which are ca. 30 nm in diameter, dispersed uniformly within the CNF matrix (Figure 1B–C) and showed well-resolved lattice fringes (Figure 1D). Interplanar spacing of the lattice fringes is 0.214 nm, corresponding to Pd_1Co_1 (111) plane of face-centered cubic (fcc) phase. Formation of a bimetallic atomic alloy of Pd and Co was confirmed by both scanning transmission electron microscopy-high-angle annular dark-field imaging (STEM-HAADF) (Figure 1E) and scanning transmission electron microscopy-energy-dispersive X-ray spectroscopy (STEM-EDX) (Figure 1F). Although the intensity of the Pd-L line is somewhat stronger than that of the Co-L line, they are similar in shape, indicating a uniform distribution of both Pd and Co atoms within the alloy NPs (Figure 1F).

By controlling the feed ratio of the metal precursors, i.e., $Pd(acac)_2$ and $Co(acac)_2$, chemical composition and size of Pd_xCo_y NPs in the CNF matrix can be easily tailored. As shown in Figure 2, uniform Pd_xCo_y alloy NPs with narrow size

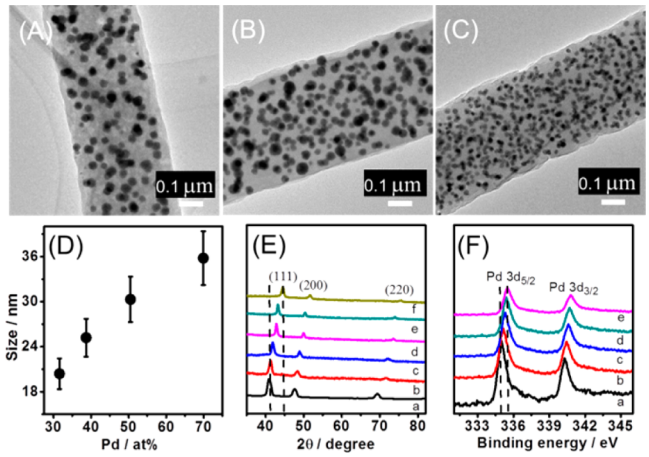

Figure 2. TEM images of Pd_2Co_1/CNF (A), Pd_3Co_2/CNF (B), and Pd_1Co_2/CNF (C). Dependence of Pd_xCo_y NP size on Pd content (D). XRD diffraction spectra (E) and Pd 3d line XPS spectra (F) for Pd/CNF, Pd_xCo_y/CNF, and Co/CNF: (a) Pd/CNF, (b) Pd_2Co_1/CNF, (c) Pd_3Co_2/CNF, (d) Pd_1Co_1/CNF, (e) Pd_1Co_2/CNF, and (f) Co/CNF.

distributions were obtained at all Pd/Co feed ratios evaluated in this study, i.e., Pd/Co = 2:1 to 1:2, and well dispersed in CNF as the matrix (see also Figures S1–S3, Supporting Information). The good dispersibility of Pd_xCo_y NPs in CNF can be attributed to the in situ simultaneous formation of Pd_xCo_y NPs and CNF during the high-temperature thermal treatment, where the bimetallic alloy NPs formed were firmly locked within the CNF structure.[17] The size of the Pd_xCo_y NPs increases almost linearly with Pd content from 19.5 nm for Pd_1Co_2 to 36.2 nm for Pd_2Co_1 (Figure 2D). This may be ascribed to the larger atomic volume of Pd (8.9 cm^3/mol) vs Co (6.7 cm^3/mol), as well as a fast crystallization rate of a Pd_xCo_y alloy with high Pd content. The chemical composition of Pd_xCo_y NPs obtained from EDX and ICP-OES agree well with the feed ratios of metal precursors (Table S1, Supporting Information). This allows for an easy control in preparation of Pd_xCo_y NPs with desired compositions.

The interplanar spacings of Pd_xCo_y (111) planes were found to be in the range of 0.211–0.217 nm (Figure S1–S3, Supporting Information), which decreases with Co content, indicating the incorporation of Co atoms into the Pd lattice and the formation of an atomic alloy.[20] The diffraction patterns of Pd_xCo_y/CNF nanocomposites are typical for fcc structures and can be assigned to (111), (200), and (220) planes (Figure 2E). As Co content increases, a gradual shift of the diffraction peaks to higher 2 values was observed, confirming the lattice contraction due to the incorporation of Co atoms. Crystal sizes estimated by Scherrer's formula are in agreement with TEM results (Table S1, Supporting Information).

Binding energies of Pd(3d) and Co(2p) for Pd_xCo_y/CNF composites, as obtained from XPS study, are comparable to those of metallic Pd and Co, respectively, indicating that both Pd and Co in Pd_xCo_y NPs are in neutral metallic state (Figures

dx.doi.org/10.1021/cs5000153 | ACS Catal. 2014, 4, 1825–1829

2F and S4, Supporting Information). Interestingly, as Co content increases in Pd_xCo_y NPs, binding energy of Pd($3d_{5/2}$) shifts to a higher value, e.g., 335.1, 335.3, 335.4, and 335.5 eV for Pd_2Co_1/CNF, Pd_3Co_2/CNF, Pd_1Co_1/CNF and Pd_1Co_2/CNF, respectively, whereas binding energy of Co($2p_{3/2}$) decreases as Pd content in Pd_xCo_y NPs increases (Figure S4, Supporting Information). The change in binding energy of Pd and Co in Pd_xCo_y NPs can be attributed to modification of the electronic structure of Pd and Co due to alloy formation.[21] The near-surface composition analysis of Pd_xCo_y NPs by XPS shows higher Pd content than the average bulk Pd content found from EDX and ICP-OES studies (Table S1, Supporting Information). This is consistent with the STEM-EDX line scan results and suggests a Pd-rich surface for the Pd_xCo_y NPs formed by high-temperature sintering.

Thus, a new type of Pd_xCo_y NP/CNF composites with Pd_xCo_y NPs uniformly dispersed and firmly embeded in CNF as the matrix has been obtained, where Pd and Co formed an atomic alloy and the size and the chemical composition of Pd_xCo_y NPs can be readily controlled. All of these features are intriguing and favorable in realizing new catalyst materials with high electrocatalytic activity and stability.

Given this, careful electrochemical and electrocatalytic studies were carried out for the resulting Pd_xCo_y NPs/CNF composites. Glassy carbon (GC) electrodes covered with Pd_xCo_y NPs/CNF composites were prepared and subjected to cyclic voltammetric (CV) cycles. It was found that the CV behavior of Pd_xCo_y NPs/CNF-modified electrodes was very similar to that of polycrystalline Pd in acid medium (Figures S5 and S6, Supporting Information); no Co dissolution signal was observed during potential cycling, indicating a good electrochemical stability of the alloy NPs in CNF due probably to the protection effect of the surface Pd-rich atomic layer. All Pd_xCo_y/CNF-modified electrodes exhibited a high electrochemical active surface area (ECSA), as estimated from the reduction charge of Pd oxide.[22] Both the onset and peak potentials for Pd_1Co_1/CNF and Pd_1Co_2/CNF electrodes shift positively, relative to those of Pd/CNF and commercial Pd/C catalysts (Figure S6, Supporting Information), which can be ascribed to a fast hydroxyl desorption from surface of Pd_xCo_y/CNF.[23] These results also show that Pd_xCo_y NPs in their composites with CNF are electrochemically accessible, which is very important for the electrocatalytic reaction.

For electrocatalytic study, formic acid and methanol were used as model compounds. Thus, by using Pd_xCo_y/CNF composite-modified GC electrodes, electrocatalytic oxidation properties of formic acid and methanol were evaluated. Figure 3A shows the CV spectra of formic acid in 0.5 M H_2SO_4 solution. A major current peak near 0.2 V can be seen, corresponding to formic acid oxidation via the direct pathway. Although Co has been known to have no electrocatalytic activity toward formic acid oxidation, the presence of Co in Pd_xCo_y alloy NPs markedly enhanced the electrocatalytic activity. The current density of the Pd_1Co_1/CNF-GC electrode is ca. 2.0 and 3.1 times that for Pd/CNF-GC and Pd/C-GC, respectively. The onset potential of formic acid oxidation is −0.103 V for the Pd_1Co_1/CNF-GC electrode, much lower than that of Pd/CNF-GC (−0.07 V) and Pd/C-GC (−0.06 V). The Pd/Co ratio in Pd_xCo_y NPs exhibited a significant effect on the electrocatalytic activity. It was found that mass activity of the catalysts for formic acid oxidation decreases in the order of Pd_1Co_1/CNF > Pd_3Co_2/CNF > Pd_2Co_1/CNF > Pd_1Co_2/CNF > Pd/CNF > Pd/C (Figure 3B). It should be noted that

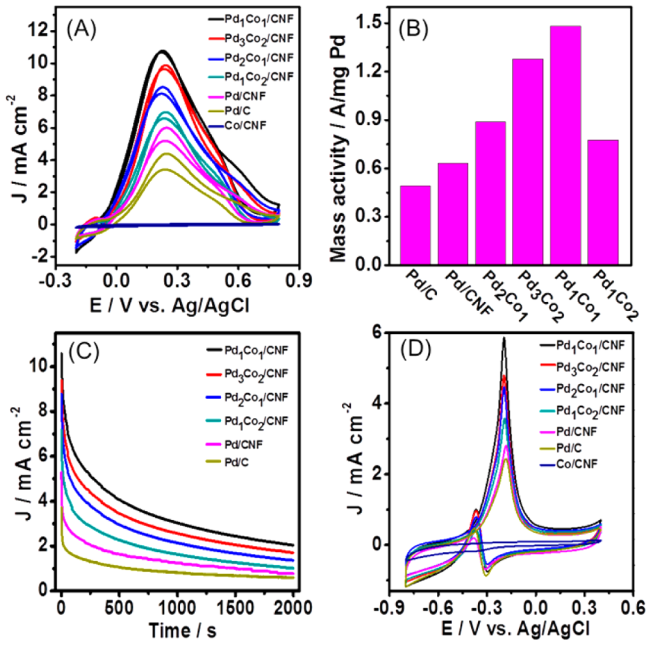

Figure 3. Pd_xCo_y NP/CNF and other electrode materials: (A) CV and (C) *i*−*t* (at 0.2 V) curves measured in 0.5 M H_2SO_4 solution containing 0.5 M HCOOH; (B) mass activity of Pd-based electrocatalysts for formic acid oxidation; (D) CV curves measured in 1 M KOH(aq) containing 1 M CH_3OH, scan rate = 50 mV/s.

Pd_1Co_1/CNF exhibits a mass activity higher than current state-of-the-art catalysts, such as Pd NPs/graphene hybrid,[24] Pt or Pt−Bi NPs loaded-OMC composite,[25] and CNT-supported Pt−Pd hollow nanosphere hybrid[26] (indexing 0.5 M HCOOH). Among Pd/C, Pd/CNF, and Pd_xCo_y/CNF prepared in this study, the Pd_1Co_1/CNF composite appears to have the best electrochemical stability, as shown from *i*−*t* curves in Figure 3C, which is consistent with CV results (Figure 3A). All of these make Pd_1Co_1/CNF composite a promising catalyst for electrocatalytic applications.

Recent studies have shown that Pd-based electrocatalysts are efficient in catalyzing methanol oxidation in alkaline medium, and may find important applications in DMFCs.[27] In comparison with Pd/C-GC and Pd/CNF-GC for methanol oxidation (Figure 3D), the Pd_1Co_1/CNF-GC electrode exhibited much better catalytic activity, as evidenced from the significantly enhanced peak current as well as the more negative onset and peak potentials. The ratio of forward anodic peak (J_f) to backward anodic peak (J_b), J_f/J_b, has been used as an important index for catalyst tolerance to poisoning. The higher the J_f/J_b ratio, the more effective poisoning species are removed from catalyst surface.[28] In this study, a J_f/J_b ratio of 4.83 was found for Pd_1Co_1/CNF-GC, which is much higher than those of commercial Pd/C catalyst (1.63) and Pd/CNF (2.33) (Figure S7, Supporting Information), indicating a better catalyst tolerance toward poisoning species for Pd_1Co_1/CNF. The mass activity of Pd_1Co_1/CNF was calculated to be 0.67 A/mg Pd, which is ca. 2.9- and 2.4-fold higher than those of the commercial Pd/C catalyst and Pd/CNF, respectively (Figure S7, Supporting Information). The mass activity of Pd_1Co_1/CNF is also higher than those reported for MWCNT/ionic liquid/Pt NPs hybrid,[29] MWCNT/PtRu NPs composite,[30] and graphene/PtPd nanodendrites hybrid[31] (indexing 1 M methanol). The variation trend of mass activity (Figures 3B and S7, Supporting Information) and stability (Figures 3C and

dx.doi.org/10.1021/cs5000153 | ACS Catal. 2014, 4, 1825−1829

S8, Supporting Information) for Pd_xCo_y NP/CNF with different Pd/Co ratios were found to be similar for both methanol and formic oxidation.

The above studies have shown that Pd_xCo_y/CNF composites prepared in this study have a good combination of properties, including excellent electrocatalytic activity, antipoisoning ability, and good stability in formic acid and methanol oxidation reactions. This can, in general, be attributed to the so-called bifunctional effect from the bimetallic Pd−Co alloy, a modified electronic structure of Pd, and the unique nanocomposite structure of Pd_xCo_y/CNF. A more detailed understanding for such good comprehensive properties of Pd_xCo_y/CNF can be as follows: (1) Co in a Pd_xCo_y alloy may facilitate oxidation of CO-like intermediates formed on nearby Pd sites through a bifunctional mechanism.[32,33] This helps to maintain free and active Pd sites for electrocatalytic reactions. (2) The down-shift of the Pd d-band in Pd_xCo_y alloy NPs relative to Pd/C and Pd/CNF (Figures 2F and S9, Supporting Information) may result in weakened adsorption of CO-like intermediates on Pd_xCo_y,[34,35] which contributes to an improved electrocatalytic activity. (3) The embeded structure of Pd_xCo_y NPs in CNF enables strong interface interaction between the two, preventing Pd_xCo_y NPs from detachment from CNF and coalescence during potential cycling. As shown in Figure S9 (Supporting Information), the Pd($3d_{5/2}$) peak of Pd/CNF (335.1 eV) appears at a higher energy level than that of Pd/C (334.9 eV), indicating an enhanced binding strength of Pd to CNF.[17] Moreover, the Pd_1Co_1/CNF-GC electrode showed no obvious decrease in ECSA after an electrochemical test (Figure S10 A, Supporting Information); no Pd_xCo_y NP aggregation or detachment was observed in the study (Figure S10 B, Supporting Information). (4) The uniform dispersion of Pd_xCo_y NPs in CNF and the fibrous network structure of Pd_xCo_y NP/CNF on an electrode allow for easy transport of electrons and access to reactants, effectively facilitating the mass transfer.

CONCLUSION

A facile preparation method for Pd_xCo_y NP/CNF nanocomposites via electrospinning followed by a thermal treatment process was successfully developed. Pd_xCo_y NPs and CNF formed simultaneously in the latter step to produce a uniform dispersion of Pd_xCo_y NPs in CNF. Structure and electrochemical properties of the resulting Pd_xCo_y NP/CNF composites were carefully studied, which showed significantly higher electrocatalytic activity and stability for Pd_xCo_y NP/CNF than commercial Pd/C catalyst and other state-of-the-art Pd- and Pt-based catalysts, particularly in formic acid and methanol electro-oxidation reactions. A dependence of electrocatalytic performance on composition of Pd_xCo_y was revealed, with the Pd_1Co_1/CNF composite being the most efficient electrocatalyst. It should be noted that free-standing films of Pd_xCo_y/CNF nanocomposites can be readily prepared and used directly as an electrode material without using any binders and conductive additives. This makes the material more attractive for fuel cell applications. The preparation method reported in this study for bimetallic Pd−Co alloy NPs/CNF composites may be applied to the preparation of other bimetallic or multimetallic alloy NP/CNF nanocomposites, thus providing a new generic approach toward highly active and stable electrocatalysts for fuel cell applications.

ASSOCIATED CONTENT

Supporting Information

Experimental and characterization details; SEM, TEM, HRTEM, STEM-HAADF images and STEM-EDX line scan profile of Pd_2Co_1/CNF, Pd_3Co_2/CNF and Pd_1Co_2/CNF nanocomposite; EDX spectrum of Pd_1Co_1/CNF nanocomposite; XPS spectra of Co 2p for Co/CNF and Pd_xCo_y/CNF nanocomposites; CV curves of Pd_xCo_y/CNF-GC, Pd/CNF-GC and Pd/C-GC electrodes in 0.5 M H_2SO_4 solution; XPS spectra of Pd 3d for Pd/CNF and commercial Pd/C catalyst; CVs of Pd_1Co_1/CNF-GC electrode before and after stability testing in 0.5 M H_2SO_4 solution; TEM image of Pd_1Co_1/CNF after stability. This material is available free of charge via the Internet at http://pubs.acs.org.

AUTHOR INFORMATION

Corresponding Author

*T. You. E-mail: youty@ciac.jl.cn.

Notes

The authors declare no competing financial interest.

ACKNOWLEDGMENTS

We are grateful for the financial support from the National Natural Science Foundation of China (No. 21222505).

REFERENCES

(1) Lamy, C.; Lima, A.; LeRhun, V.; Delim, F.; Coutanceau, C.; Leger, J. M. *J. Power Sources* **2002**, *105*, 283−296.
(2) Rice, C.; Ha, S.; Masel, R. I.; Waszczuk, P.; Wieckowski, A.; Barnard, T. *J. Power Sources* **2002**, *111*, 83−89.
(3) Antolini, E. *Energy Environ. Sci.* **2009**, *2*, 915−931.
(4) Bianchini, C.; Shen, P. K. *Chem. Rev.* **2009**, *109*, 4183−4206.
(5) Park, S.; Xie, Y.; Weaver, M. J. *Langmuir* **2002**, *18*, 5792−5798.
(6) Stamenkovic, V. R.; Mun, B. S.; Arenz, M.; Mayrhofer, K. J. J.; Lucas, C. A.; Wang, G. F.; Ross, P. N.; Markovic, N. M. *Nat. Mater.* **2007**, *6*, 241−247.
(7) Shao, M. H.; Sasaki, K.; Adzic, R. R. *J. Am. Chem. Soc.* **2006**, *128*, 3526−3527.
(8) Wang, D. L.; Xin, H. L.; Yu, Y. C.; Wang, H. S.; Rus, E.; Muller, D. A.; Abruña, H. D. *J. Am. Chem. Soc.* **2010**, *132*, 17664−17666.
(9) Mazumder, V.; Chi, M. F.; Mankin, M. N.; Liu, Y.; Metin, O.; Sun, D. H.; More, K. L.; Sun, S. H. *Nano Lett.* **2012**, *12*, 1102−1106.
(10) Chen, L. Y.; Guo, H.; Fujita, T.; Hirata, A.; Zhang, W.; Inoue, A.; Chen, M. W. *Adv. Funct. Mater.* **2011**, *21*, 4364−4370.
(11) Stein, A.; Wang, Z. Y.; Fierke, M. A. *Adv. Mater.* **2009**, *21*, 265−293.
(12) Gasteiger, H. A.; Kocha, S. S.; Sompalli, B.; Wagner, F. T. *Appl. Catal., B* **2005**, *56*, 9−35.
(13) Sun, S. H.; Zhang, G. X.; Geng, D. S.; Chen, Y. G.; Li, R. Y.; Cai, M.; Sun, X. L. *Angew. Chem., Int. Ed.* **2011**, *50*, 422−426.
(14) Wu, B. H.; Hu, D.; Kuang, Y. J.; Liu, B.; Zhang, X. H.; Chen, J. H. *Angew. Chem., Int. Ed.* **2009**, *48*, 4751−4654.
(15) Hsin, Y. L.; Hwang, K. C.; Yeh, C. T. *J. Am. Chem. Soc.* **2007**, *129*, 9999−10010.
(16) Wang, Y.; Guo, C. X.; Wang, X.; Guan, C.; Yang, H. B.; Wang, K.; Li, C. M. *Energy Environ. Sci.* **2011**, *4*, 195−200.
(17) Wu, Z. X.; Lv, Y. Y.; Xia, Y. Y.; Webley, P. A.; Zhao, D. Y. *J. Am. Chem. Soc.* **2012**, *134*, 2236−2245.
(18) Matsumoto, T.; Komatsu, T.; Nakano, H.; Arai, K.; Nagashima, Y.; Yoo, E.; Yamazaki, T.; Kijima, M.; Shimizu, H.; Takasawa, Y.; Nakamura, L. *Catal. Today* **2004**, *90*, 277−281.
(19) Wang, D.; Li, Z. C.; Chen, L. W. *J. Am. Chem. Soc.* **2006**, *128*, 15078−15079.
(20) Fernández, J. L.; Walsh, D. A.; Bard, A. J. *J. Am. Chem. Soc.* **2005**, *127*, 357−365.

(21) Wang, H.; Wang, A. Q.; Wang, X. D.; Zhang, T. *Chem. Commun.* **2008**, 2565−2567.
(22) Xiao, L.; Zhuang, L.; Liu, Y.; Lu, J. T.; Abruna, H. D. *J. Am. Chem. Soc.* **2009**, *131*, 602−608.
(23) Peng, Z. M.; Yang, H. *J. Am. Chem. Soc.* **2009**, *131*, 7542−7543.
(24) Yang, J.; Tian, C. G.; Wang, L.; Fu, H. G. *J. Mater. Chem.* **2011**, *21*, 3384−3390.
(25) Ji, X. L.; Lee, K. T.; Holden, R.; Zhang, L.; Zhang, J. J.; Botton, G. A.; Couillard, M.; Nazar, L. F. *Nat. Chem.* **2010**, *2*, 286−293.
(26) Liu, B.; Li, H. Y.; Die, L.; Zhang, X. H.; Fan, Z.; Chen, J. H. *J. Power Sources* **2009**, *186*, 62−66.
(27) Zhang, J.; Huang, M.; Ma, H.; Tian, F.; Pan, W.; Chen, S. *Electrochem. Commun.* **2007**, *9*, 1298−1304.
(28) Chen, Y. X.; Miki, A.; Ye, S.; Sakai, H.; Osawa, M. *J. Am. Chem. Soc.* **2003**, *125*, 3680−3681.
(29) Chu, H. B.; Shen, Y. H.; Lin, L.; Qiu, X. J.; Feng, G.; Lin, Z. Y.; Wang, J. Y.; Liu, H. C.; Liu, Y. *Adv. Funct. Mater.* **2010**, *20*, 3747−3752.
(30) Chetty, R.; Xia, W.; Kundu, S.; Bron, M.; Reinecke, T.; Schuhmann, W.; Muhler, M. *Langmuir* **2009**, *25*, 3853−3860.
(31) Guo, S. J.; Dong, S. J.; Wang, E. K. *ACS Nano* **2009**, *4*, 547−555.
(32) Watanabe, M.; Motoo, S. *J. Electroanal. Chem.* **1975**, *60*, 267−273.
(33) Hsieh, C. T.; Lin, J. Y. *J. Power Sources* **2009**, *188*, 347−352.
(34) Derry, G. N.; Ross, P. N. *Solid State Commun.* **1984**, *52*, 151−154.
(35) Ruban, A.; Hammer, B.; Stoltze, P.; Skriver, H. L.; Nørskov, J. K. *J. Mol. Cata. A-Chem.* **1997**, *115*, 421−429.